Peer-reviewed version available at Appl. Sci. 2019, 9, 3528; doi:10.3390/app9173528

*Article*

# GaN/$Ga_2O_3$ Core/Shell Nanowires Growth: Nanostructures for Future CO-Sensors Developments

**Q.C. Bui, L. Largeau, M. Morassi, N. Jegenyes, O. Mauguain, L. Travers, X. Lafosse, C. Dupuis, J.C. Harmand, M. Tchernycheva and N. Gogneau ***

Centre de Nanosciences et de Nanotechnologies—CNRS-UMR9001, Université Paris-Sud, Université Paris-Saclay, 10 Boulevard Thomas Gobert, F-91120 Palaiseau, France; shiningskill@gmail.com(Q.C.B.); ludovic.largeau@c2n.upsaclay.fr (L.L.); martina.morassi@c2n.upsaclay.fr (M.M.); jegenyes@free.fr (N.J.); olivia.mauguin@c2n.upsaclay.fr (O.M.); laurent.travers@u-psud.fr (L.T.); xavier.lafosse@c2n.upsaclay.fr (X.L.); christophe.dupuis@c2n.upsaclay.fr (C.D.); jean-christophe.harmand@c2n.upsaclay.fr (J.C.H); maria.tchernycheva@u-psud.fr (M.T.)

* Correspondence: noelle.gogneau@c2n.upsaclay.fr; Tel.: +33-(0)1-70-27-05-49

**Abstract:** The development of sensors for monitoring Carbon Monoxide (CO) in a large range of temperature is of crucial importance in areas as monitoring of industrial processes or personal tracking using smart objects. Devices integrating GaN/$Ga_2O_3$ core/shell nanowires (NWs) is a promising solution allowing combining the high sensitivity of the electronic properties to the states of GaN-core surface; and the high sensitivity to CO of $Ga_2O_3$-shell. Because the performances of sensors primarily depend on the material properties composing the active layer of the device, it is essential to control these properties and in first time its synthesis. In this work, we investigate the synthesis of GaN/$Ga_2O_3$ core-shell NWs with a special focus on the formation of the shell. The GaN NWs grown by Plasma-assisted molecular beam epitaxy, are post-treated following thermal oxidation to form $Ga_2O_3$-shell surrounding the GaN-core. We establish that the $Ga_2O_3$-shell thickness can be modulated from 1 up to 14 nm by changing the oxidation conditions, and follows the diffuse-controlled reaction. By combining XRD-STEM and EDX analysis, we also demonstrate that the oxide shell formed by thermal oxidation is crystalline and presents the β-$Ga_2O_3$ crystalline phase, and is synthesized in epitaxial relationship with the GaN-core.

**Keywords:** core/shell nanowires; GaN; $Ga_2O_3$; metal-oxide semiconductor; gas sensor devices

## 1. Introduction

The rapid development of smart objects has led to the increased interest of sensor technologies, which enable the collection and exchange of sensed data in real-time. With the development of nanotechnologies, the sensor efficiency and accuracy have been improved and thereby the application domains have been largely extended [1,2]. Among a very wide range of sensor applications, such as intelligent building, public safety or environmental monitoring, the development of sensor devices allowing monitoring of the harmful Green House Gases (GHGs) is of the utmost importance. GHGs need to be monitored in areas as diverse as monitoring of industrial processes or personal tracking using smart objects. The Carbon Monoxide (CO) is one of GHGs. Its efficient detection and monitoring is essential and require the development of specific sensor devices which must be reliable, responsive, highly sensitive, miniaturized, low cost, and capable to operate on a large range of temperature, from ambient temperatures (smart objects) to high temperatures (up to 600°C for industrial combustion processes).

The sensing and data collection of gases such as CO, but also such as $CO_2$ or NOx, require the sensor to fulfill four main criteria: 1- The sensitivity with a minimum of detection of the order of few ppm (an even ppb for harmful gases, e.g. $NO_x$) for precisely monitoring the combustion process, a high response rate and a fast recovery time to initial state; 2) The selectivity to monitor targeted gas without cross-interference with other gases, whose presence should not affecting the detection signal

quality (i.e. sensitivity), the response rate and recovery time; 3) The sensing stability (by keeping high selectivity), and reliability in harsh environment (environmental humidity, pressure, radiation and/or chemical attack); and 4) The miniaturization and manufacturability of sensor device to combine an integration of multi-sensing devices (i.e. simultaneous gas detection) with the lowest power consumption in order to develop ultra-compact self-powered sensors.

Most of actual sensors are solid-state sensors based on the interaction of gas particles with surfaces and volumes. The electrochemical potential, the resistivity, the density, and/or the optical properties are altered upon gas adsorption, which must be maximized in order to increase the reaction and therefore the detection. Common high-temperature GHG sensors are based on metal oxide material working on the principle of chemiresistor. For CO, the detection mechanism is based on the redox reaction between the gas species and the pre-adsorbed $O_2$ on the surface of metal oxide, affecting the depletion layer and thus resulting in the change of the conductivity of the material [3-7].

Metal oxide sensors based on $SnO_2$ material have been developed to monitor CO due to their relatively high sensitivity [8-9]. Indeed, the detection of 5 ppm CO in few seconds at 300 °C has been demonstrated [10-11]. Chemiresistor sensors based on Titanium Oxide ($TiO_2$)/lanthanum oxide ($La_2O_3$/CuO) have also demonstrated their capacity to selectively detect down to 500 ppm of CO against $CH_4$ [12] under 5% of $O_2$ up to 600 °C. However, these kind of sensors can present a low selectivity (due to interference with other gas), a drift of the sensor response and/or a poor recovery. CO-sensors based on $Ga_2O_3$ thin film have also been developed usually operating in the 400-600°C temperature range. Comparing to $SnO_2$, $Ga_2O_3$ gas sensor present faster response, faster recovery time and lower cross-sensitivity to humidity [13-16]. The sensitivity and selectivity performances of these $Ga_2O_3$ sensors have been improved by adjusting the oxygen vacancy concentration [17] or by using gold particles to catalyze the reaction between adsorbed oxygen on sensor surface and gas molecule by reducing their activation energy [18]. However, these sensors based on planar films present numerous drawbacks. Among them, the limited surface, where takes place the interaction between gas molecules and materials, results in limited sensor performances.

This last decade, a new class of sensors based on 1D-nanstructures, such as nanowires (NWs) or nanorods (NRs), has appeared as a promising way to improve the sensing performances. Thanks to their specific properties, these 1D-nanostructures present, in comparison with their 2D-film counterparts, important characteristics to fundamentally improve the gas-sensing efficiency in terms of sensitivity, response and spatial resolution [19-28]: (i) their large surface to volume ratio greatly enhances the detection limit and thus leads to a higher sensitivity [29], and induces enhanced and tunable surface reactivity implying possible room temperature operation, faster response and recovery time; (ii) their nanometer scale dimensions are compatible with the size of species being sensed, opening up the way for nano-detection; and finally (iii) due to these morphological properties combined with their quasi-lattice perfection, the NWs offer superior mechanical properties leading to large elastic deformation without plastic deformation or fracture [30], higher flexibility, higher robustness and higher resistance to fatigue, then extending the operational lifetime of nano-systems [31].

As for 2D based sensors, the main materials used for developing gas-sensors, from room temperature to 400°C, are chemiresistor based on metal oxide NWs such as $SnO_2$, ZnO, $In_2O_3$ and $Ga_2O_3$. However, in spite of the considerable effort devoted to develop high-efficient gas sensors based on 1D-nanostructures, further improvements of the sensor performances are today needed including sensitivity, low detection limit, response-recovery time, selectivity as well as operating temperature range.

To enhance the sensing performances, several approaches have been considered to modify the surface properties, such as doping, surface functionalization or hybridization [23] and core-shell heterostructures [23, 32]. Concerning this last approach, carbon nanotubes-core/vanadium oxide-shell [33], $Ga_2O_3$- core/$SnO_2$-shell NWs [34], ZnO-core/$Co_3O_4$-shell NWs [35], Pb/$In_2O_3$ nanocubes [36] and $Ga_2O_3$-core/GaN-shell NWs [37] have demonstrated enhanced sensing performances or sensing at a lower operating temperature. In these heterostructures, the sensing is based on the NW resistance

modulation before and after exposing it to gas such as CO. The core-shell NW heterostructures are characterized by the existence of two depletion zone, a first one at the air/shell interface and a second one at the shell/core interface [37]. The adsorption/desorption of the gas on the heterostructure surface modifies the depth of the first depletion layer, which in turn alters the second one at the interface and thus induces a modulation of the corresponding potential barrier height. Carrier transport is thus affected, resulting in a large change in resistance and thus in an enhanced response of the core/shell NW sensor. Based on this mechanism, $Ga_2O_3$/GaN core/shell based sensor has demonstrated detection of 10–200 ppm CO at 150°C with the responses were 1.6-3.1 times stronger than a pure $Ga_2O_3$ nanowire sensor [37]. In spite of these encouraging results, the system presents a strong response to other gases, which indicates its poor selectivity to CO.

To develop highly sensitive and selective CO-gas sensor device operating in a large range of temperature, from ambient temperature (smart object) to high temperature (up to 600°C for industrial combustion processes), we propose to consider GaN/ $Ga_2O_3$ core-shell NW heterostructures combining the advantages of the GaN-core and $Ga_2O_3$-shell materials. GaN and its alloys present favorable properties to develop gas-sensors and especially in playing the NW-core role: (i) the III-Nitrides present high thermal and chemical stability as well as radiation hardness, thus allowing their use in harsh environments; (ii) they exhibit less intrinsic leakage and are capable of operating at high temperatures due to the larger bandgap and stronger bond energy [38]; (iii) the GaN ,as same as AlN, have a high Pauling Electronegativity difference (1.23 eV), which confers a high sensitivity of the electronic properties to the state of its surface (K Parameter) [38]; and (iv) the nitrides are characterized by conductivity in the range of $10^{-8}$ to $10^{3}$ S/cm, allowing both to keep the influence of the surface on the charge carriers and the modulation of the Fermi level [38]. The choice of $Ga_2O_3$-shell is motivated by the following advantages: (i) $Ga_2O_3$ present high thermal stability, especially the β-$Ga_2O_3$ crystalline phase (the most stable phase). This property is suitable to be used for sensing CO in high temperature environment of industrial factory; (ii) $Ga_2O_3$ presents high sensitivity to CO. In fact, its resistivity is very sensitive to CO at high temperature. Thus by measuring and analyzing the changing in resistance of $Ga_2O_3$ shell, it is possible to detect CO species [39]; (iii) Presence of $Ga_2O_3$ layer covering the GaN surface, resulting from oxidation mechanism upon contact to ambient air atmosphere, increases the response of GaN sensors to CO [38].

Because the performances of sensors primarily depend on the material properties composing the active layer of the device, it is of crucial importance to control these properties and in first time its synthesis. In this paper, we investigate the synthesis of GaN/$Ga_2O_3$ core-shell NWs with a special focus on the formation of the $Ga_2O_3$ shell. The GaN nanowires grown by Plasma-assisted molecular beam epitaxy (PA-MBE), are post-treated following thermal oxidation to form $Ga_2O_3$ shell surrounding the GaN core. We established that the thickness of the $Ga_2O_3$ shell can be modulated by changing the oxidation conditions (temperature, $O_2$ flux and time of oxidation ), from 1 up to 14 nm and follows the diffuse-controlled reaction. The structural properties of the shell have been investigated by combining XRD, TEM-STEM and EDX. Then, we have demonstrated that the oxide shell formed by thermal oxidation is crystalline and presents the β-$Ga_2O_3$ crystalline phase, the most stable one, and is synthesized in epitaxial relationship with the GaN core.

## 2. Materials and Methods

The synthesis of GaN/$Ga_2O_3$ core-shell NW heterostructures is composed of two successive steps:

*1- GaN-core NW growth:* Self-assembled free-catalyst GaN-core NWs were grown on conductive oxide-free Si (111) substrate (resistivity of the order of 0.007 Ω cm) in a molecular beam epitaxy chamber (MBE) (RIBER Compact 12 PA-MBE system, Bezons, France), equipped with a radio-frequency N plasma source. After a chemical cleaning and a thermal deoxidation of the substrate surface to remove the organic pollutants and the native oxide, a 2.5-nm-thick AlN buffer layer was deposited at 620°C following a previously reported procedure [40]. This seed layer allows a better control of the NW nucleation and density, a reduction of the NW twist and an improvement of the

Peer-reviewed version available at Appl. Sci. 2019, 9, 3528; doi:10.3390/app9173528



NW vertical orientation [41-44]. Then, the temperature is ramped to 790°C to grow the GaN NWs under nominally N-rich conditions with an N/Ga flux ratio of 1.36. Following this growth procedure, the GaN NWs are vertically oriented with a hexagonal shape delimited by [10-10] plane, are characterized by a quasi-crystalline perfection (absence of dislocations) [40], a prevalent N-polarity [45-46] and present reproducible dimensions and densities (Fig. 1). GaN NWs considered in this study are characterized by a density of $5.10^9$ NW/cm², an average diameter of 40 ± 5 nm and average height of 650 ± 100 nm, these structural characteristics being extracted from high-resolved SEM images.

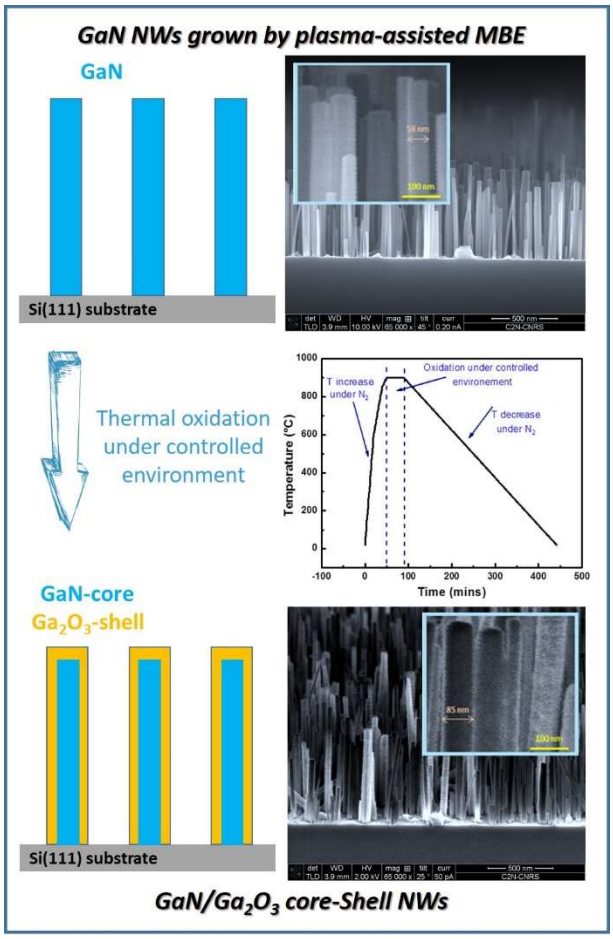


**Figure 1.** Schematization and SEM images of GaN NWs before and GaN/$Ga_2O_3$ core-shell NWs after oxidation. The cycle of oxidation is also schematized.

2- *$Ga_2O_3$ shell synthesis:* The $Ga_2O_3$ shell is formed around GaN NW by thermal oxidation post-treatment. The as-grown GaN NWs are oxidized at high temperature following the procedure described in Fig. 1. The adjustment of the temperature to the oxidation one is performed under Nitrogen to avoid any alteration of the NW surfaces. After the stabilization of the oxidation temperature, the controlled environment is injected and the oxidation time is considered. Finally, the temperature is decreased under Nitrogen to the ambient one. During the oxidation step, due to the high temperature, the GaN is decomposed at the surface. The Nitrogen is removed in the environment, while the Ga, with its free dangling bonds is linked with oxygen, then forming $Ga_2O_3$ oxide (Fig. 1). After the first oxide monolayer is formed, it will separate the oxygen and the GaN creating a barrier. To continue the oxidation, the oxygen species should diffuse through the $Ga_2O_3$ oxide to form another oxide monolayer. As a function of the oxidation time, the shell surrounding the GaN core becomes thicker.

The oxidation mechanisms, the rate of oxidation, the quality of $Ga_2O_3$ layer and the interface GaN/$Ga_2O_3$ can be affected by many factors such as: temperature, oxidized agents and their flow rate,

pressure, GaN structure and concentration of impurities, etc. In order to investigate the formation of the $Ga_2O_3$-shell, the oxidation of GaN-core NWs has been tested under different conditions: oxidation time, temperature and $N_2/O_2$ ratio, summarized in Table 1. We note here that the $N_2/O_2$ ratio was chosen to be approximately equivalent to the normal air composition. The "humid" term refers to oxidation environment equivalent to normal air (i.e. with water vapor), while the "dry" term refers to the same oxidation conditions ($N_2/O_2$ ratio) but without water vapor.

**Table 1.** Conditions of oxidation.

| Series \ Factor | Temperature (°C) | $O_2$ flux (sccm) | $N_2$ flux (sccm) | Time (min) |
|---|---|---|---|---|
| 1 | 900 | 1.3 *dry atmosphere* | 5 | 5 - 15 |
| 2 | 900 | 1.3 *humid atmosphere* | 5 | 3 - 15 |
| 3 | 850 | 1.3 *dry atmosphere* | 5 | 7 – 30 |
| 4 | 850 | 0.4 – 1.3 *dry atmosphere* | 5 | 15 |

The structural properties of the core-shell NWs have been characterized by combining different techniques, such as Scanning Electron Microscope (SEM), Transmission Electron Microscope (TEM), X-Ray Diffraction (XRD) and Energy Dispersive X-ray (EDX). To evaluate the shell formation, the diameters of NWs were systematically characterized before and after each oxidation by High Resolution SEM images in cross-section view (SEM Magellan 400L-FEI) and confirmed by STEM/EDX analysis. The crystal structure of NWs was analyzed by X-Ray Diffraction with a Smartlab RIGAKU under in-plane diffraction configurations. The choice of this experimental configuration is motivated by the thinness of the sample (the average height of the NW being of 650 nm) and the study of the parallel plan to the c-axis of the vertically oriented NWs on Si(111) substrate. Finally, the composition and crystal structure of samples after oxidation were analyzed by using high-resolved transmission electron microscope having the possibility to work also under the scanning TEM mode and the energy dispersive X-ray mode (EDX).

## 3. Results and Discussion

In order to adjust the performances of sensors based on GaN/$Ga_2O_3$ core-shell NW, it is of crucial importance to understand the conditions of the shell formation and thus to control its thickness and crystalline quality. The main factors driving the thermal oxidation of GaN NWs are: The temperature, the $O_2$ flux, the time and the dry/humid environment. The effects of these factors were studied through different series of samples (Table 1). In order to thoroughly investigate the formation of the oxide shell, we have combined various techniques of characterization allowing us to access to the morphology modification of the NWs, as well as the composition and crystallographic phase of the oxide shell.

### *3.1. $Ga_2O_3$ shell thickness evolution*

By comparing the HR-SEM images of NWs before and after the oxidation, we can observe that the as-grown MBE GaN-core NWs are characterized by smooth surfaces, while the GaN/$Ga_2O_3$ core-shell NW heterostructures present rough surfaces (Figure 1). The formation of $Ga_2O_3$ shell is also characterized by an increase of the NW diameter. Due to the self-assembled growth mode of the NWs (cf. Materials and Methods), we have a modulation of the as-grown NW diameter from wire to wire. To realize a representative study, each sample has been measured before and after oxidation with a statistical analysis of the NW diameter based on the measurement of a large number of nanostructures (around 400 NWs). The diameter follows a single Gaussian distribution, within the limits of statistical error and the error bars correspond to the full width at half maximum of the Gaussian fit in each case (Figure 2a). The shell thickness is estimated from the increase of the NW

diameter after oxidation was evaluated by the difference between mean values of two distributions with standard error calculated as follows: $\sigma_{2-1} = \sqrt{\frac{\sigma_1^2}{N_1} + \frac{\sigma_2^2}{N_2}}$.

The diameter expansion is caused by the difference between the specific volume of the GaN (13.5 $cm^3/mol$) and the β-$Ga_2O_3$ (31.8 $cm^3/mol$). Then, when a Ga atom of GaN is converted to a Ga atom of $Ga_2O_3$, the corresponding volume increases. The specific volume of GaN and β-$Ga_2O_3$ have been calculated based on their molar mass and densities (for GaN: 83.7 g/mol and 6.2 $g/cm^3$ [47]; for β-$Ga_2O_3$ 187.4 g/mol and 5.9 $g/cm^3$ [48]). Therefore, the diameter of GaN NWs is expected to be expanded after the oxidation. We want to note that even if the formation of the oxide mainly explains the expansions of the NW diameter, other reasons can accompany this one, such as the non-uniform oxidation, the defects of $Ga_2O_3$ structure, the vacancies in the shell, etc. It should also be noted that the difference between the mean values of the two distributions before and after the oxidation is the average expansion of the NW diameter. However, it is not exactly equivalent to 2 times the thickness of the formed oxide. In fact, when GaN is oxidized, a layer of GaN at the side of the NW is converted into the oxide layer. This means that the oxide thickness is equal to the thickness expansion plus the thickness of GaN layer that has been oxidized, as schematized on Figure 2d.

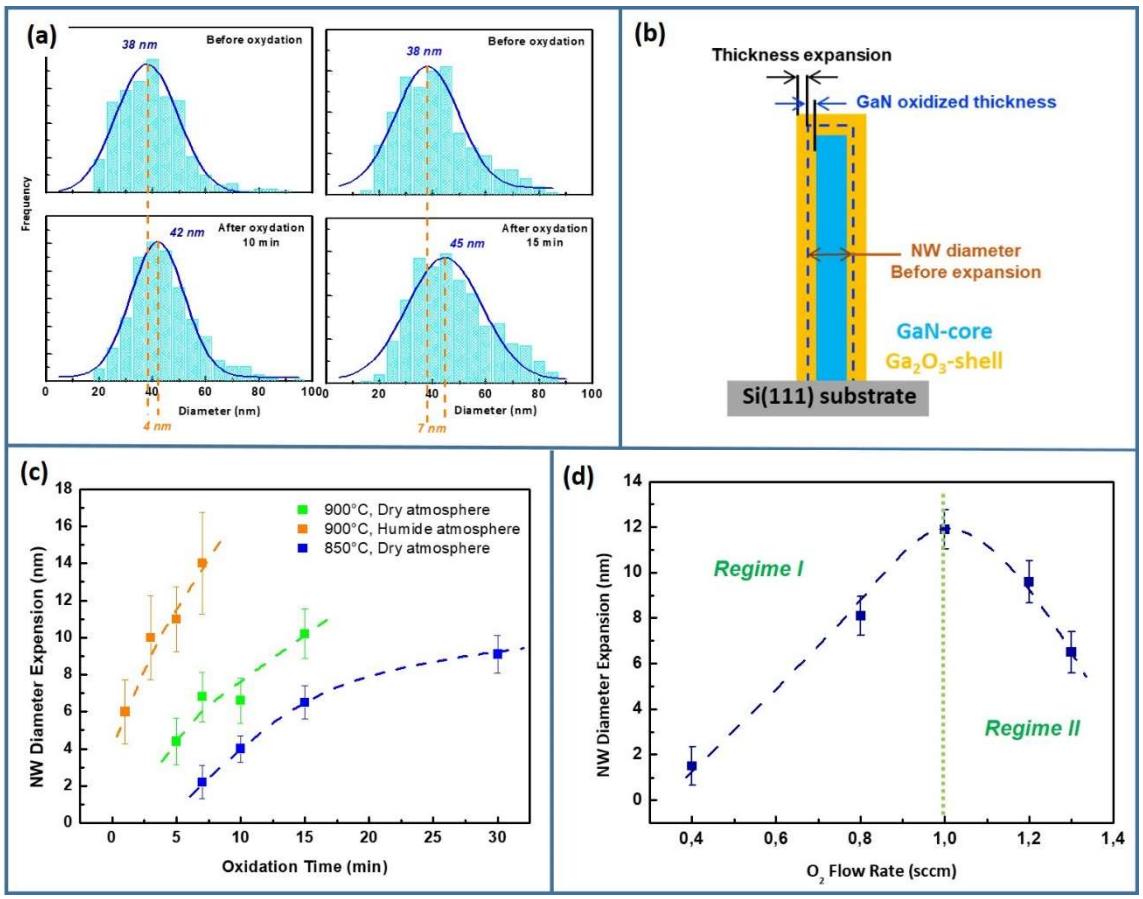


**Figure 2. (a)** Gaussian distribution of the NWs diameter before and after oxidation during 10 min and 15 min under a dry atmosphere at 850°C for 1.3 sccm of $O_2$, 5 sccm of $N_2$. The diameter expansion is schematized with dashed lines; **(b)** Schematization of the NW expansion; **(c)** NW diameter expansion as a function of the oxidation time for 1.3 sccm of $O_2$ and 5 sccm of $N_2$, for different temperatures and atmospheres; **(d)** NW diameter expansion as a function of the $O_2$ flux for a fixed temperature of 850°C, a $N_2$ flux of 5 sccm, an oxidation time of 15 min and under dry atmosphere.

Figure 2 establishes the direct correlation between the diameter expansion and the oxidation conditions. We can observe that the $Ga_2O_3$ shell thickness can be controlled between 1 and 14 nm as a function of the oxidation conditions. Figure 2c shows the diameter expansion at 850°C (blue curve) and 900°C (green curve) as a function of the oxidation time, for $O_2$ and $N_2$ fluxes of 1.3 sccm and 5

sccm respectively and under dry atmosphere (Table 1, Series 1 and 3). The diameter expansion due to the oxidation of the GaN NWs increases with time, indicating that the NWs keep continue to be oxidized with time. The diameter expansion of the samples oxidized at 900°C is always higher than the one occurring at 850°C for the same conditions and time of oxidation. This result demonstrates that the oxidation rate was faster with higher temperature. These results are similar to ones reported in [49-52]. The curve corresponding to the oxidation temperature of 850°C in figure 2c shows that the diameter expansion (or the increase of the oxidation rate) becomes slower with time. This phenomenon indicates that the oxidation follows the diffuse-controlled reaction. This means that the formed oxide layer starts to be thick enough to hinder the interaction between the GaN and the oxygen. The decrease of the oxidation rate in time is not observed in samples oxidized at 900°C, despite a thicker oxide layer as evidenced by the higher diameter expansion. This behavior can be explained by the higher oxidation temperature. In fact, at higher temperature, the system is more reactive and the diffusion of oxygen through the oxide layer is easier and faster. We can then assume an under-linear thickening of the shell for higher oxidation times.

Now, we compare the diameter expansion as a function of the time for the same oxidation conditions (T = 900°C, $O_2$ = 1.3 sccm, $N_2$ = 5 sccm), but for different atmospheres, i.e. under dry (green curve) and wet (orange curve) thermal oxidation conditions. The comparison between oxidized samples shows that the diameter expansion of NWs oxidized in wet atmosphere is more important. In other words, it indicates that the oxidation rate is faster under humid environment. However, the faster oxidation yields a more difficult control over the oxide formation and as reported in the literature, leads to a poor GaN/ $Ga_2O_3$ interface causing unstable electrical properties of the structure [15]. Thus, these conditions are undesirable since they can degrade the sensor performances.

Finally, we have analyzed the oxidation under dry atmosphere as a function of the $O_2$ flux (varying between 0.4 and 1.3 sccm), by keeping content the temperature at 850°C, the $N_2$ flux at 5 sccm and the oxidation time at 15 min. We can observe on Figure 2d two different regimes of oxidation rate: The Regime I is characterized by a continuous increase of the oxidation rate with the $O_2$ flux, while in Regime II, the oxidation rate decreases for high fluxes. To understand the origin of these two regimes, we have to consider that the variation of oxygen flow rate can affect many factors during the oxidation, such as the concentration of oxygen and nitrogen, the total pressure in the oxidation chamber, as well as the partial pressure of oxygen and nitrogen.

The nitrogen is an inert gas, so that it is not participating to the oxidation reaction. By contrast, the increase of the oxygen flow induces an increase of the oxygen concentration in the $N_2/O_2$ gas mixture, and thus of the partial pressure of oxygen ($N_2$ flux being kept constant), leading to a faster diffusion of oxygen through the being-formed oxide shell. Thus, the oxidation rate is enhanced. From the GaN decomposition point of view, when the sample is oxidized in environment with low oxygen flow rate, partial pressure of nitrogen is high, which can reduce the decomposition of GaN as mentioned in report [14]. In other words, the decomposition of GaN gets faster as the oxygen flow rate becomes higher and the partial pressure of nitrogen becomes lower. These behaviors are both in good agreement with the diameter expansion observed in Regime I where the oxygen flow rate increases from 0.4 to 1.0 sccm. However, for fluxes higher than 1.0 sccm, the diameter expansion decreases. This behavior can appear contradictory to the last described one. To explain the Regime II behavior, the increase of the total pressure with the oxygen flow rate can be considered. This means that the GaN decomposition could be more difficult under high pressure, resulting in a slower oxidation rate. Additional experiments are needed to understand this Regime II behavior. Nevertheless, the less pronounced oxidation rate for higher fluxes does not prevent the control of the $Ga_2O_3$ shell thickness from 1 to 14 nm by adjusting the oxidation temperature, time and atmosphere as illustrated by Figure 2c, where the $O_2$ flux was fixed to 1.3 sccm, the highest tested one (Figure 2d).

### *3.2. Structural characterization of the $Ga_2O_3$ shell*

To study the composition and the crystal structure of the $Ga_2O_3$ oxide shell, samples have been characterized by combining X-Ray diffraction, STEM and EDX.

Figure 3 shows typical spectra of GaN (Figure 3a) before oxidation and GaN/$Ga_2O_3$ NWs (Figure 3c) after oxidation, analyzed by XRD using in-plane Phi/2ThetaChi scan configuration. The spectra performed on as-grown GaN NWs show only 2 peaks located at 47.3° and at 57.8° corresponding respectively to the signal of Si (220) and the signal of hexagonal GaN (11-20). By contrast, the spectrum of GaN NWs after oxidation present two additional peaks, located at 61.1° and 64.4°, suggesting the signals of oxide. According to reports [50-51], monoclinic β-$Ga_2O_3$ phase, the most stable one, appears after similar oxidation process of GaN. By comparing with the reference XRD spectra of β-$Ga_2O_3$ shown in figure 3b [53], the peak at 61.1° is attributed to the signal of β-$Ga_2O_3$ (020), as confirmed by STEM analysis (presented after), while the one around 64° is assigned to the signal of β-$Ga_2O_3$ (403).

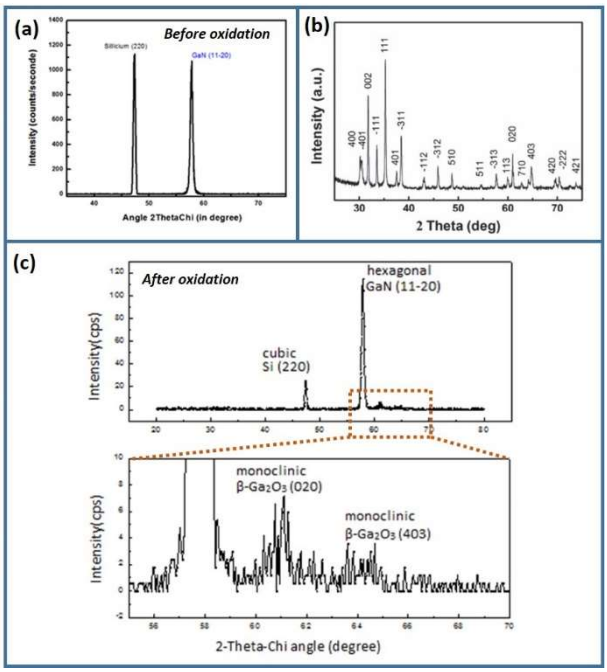


**Figure 3.** XRD analyze using in-plane Phi/2ThetaChi scan configuration. **(a)** XRD spectra of as-grown GaN NWs before thermal oxidation; **(b)** Reference XRD spectrum of the β-$Ga_2O_3$ in report [53]; **(c)** XRD spectra of GaN/$Ga_2O_3$ NWs after oxidation at 900°C during 7 min under dry atmosphere with $N_2$ and $O_2$ fluxes of 5 sccm and 1.3 sccm respectively.

We note here that only the GaN (11-20) peak appears on figures 3a and 3c. The peak of GaN (10-10) at 32.3903° does not appear, despite it is perpendicular to the sample surface and thus can give signal in XRD in-plane scanning. However, in XRD phi/2thetachi mode scanning, to observe several signatures in the same spectrum, the planes must be parallel to each other. The plane (11-20) cannot be parallel to the plane (10-10) in same NW as the structure grown by PA-MBE is monocrystalline with a unique orientation for the whole NW ensemble. The missing of GaN (10-10) peak in figure 3 shows that the samples do not present NW in position where its plane (10-10) is parallel to the (11-20) one, and thus demonstrate that NWs have preferentially orientation as we have previously demonstrated [44].

The detailed positions of peaks for three different samples before and after dry oxidation are showed in the Table 2. The theoretical values of 2ThetaChi have been calculated by using theoretical parameters of crystal.

**Table 2.** 2ThetaChi values of crystals.

| | Si (220)[1] | GaN (11-20) | $Ga_2O_3$ (020) | $Ga_2O_3$ (403) |
|---|---|---|---|---|
| T=900°C, $N_2/O_2$=5/1.3, Time=7min, Shell thickness=6.9 | 47.3516° | 57.8236° | 61.0465° | 64.6155° |
| T=850°C, $N_2/O_2$=5/1.3, Time=15min, Shell thickness=6.5 | 47.3277° | 57.8005° | 61.0825° | 64.0635° |
| T=850°C, $N_2/O_2$=5/0.8, Time=15min, Shell thickness=8.1 | 47.3262° | 57.8005° | 61.0400° | 64.4000° |
| Pure GaN NWs | 47.3211° | 57.7507° | | |
| Theory 2ThetaChi | 47.3010° | 57.7742° | 60.8969° | 64.6319° |

[1] Because the crystal parameters remain unchanged after oxidation process as explained below, the Si peak is considered to compare values of GaN and Ga2O3 in the different samples.

The mismatch existing between GaN and $Ga_2O_3$ at the core-shell interface induces internal strain and thus affects their parameters as well as values of 2ThetaChi in XRD spectra. Due to the specific volume of GaN and $Ga_2O_3$, from a theoretical point of view, $Ga_2O_3$ should induce stretching in the GaN, and reciprocally, GaN should induce compression on $Ga_2O_3$. This strain equilibrium depends on the thickness ratio between core and shell. By regarding the thickness of the GaN-core (diameter ~ 40 nm) and of the oxide shell (for thickness < 10 nm), the main stress expressed in the heterostructure is localized in the shell, as demonstrated by the material crystal parameters extracted from XRD measurements, summarized in the Table 3. The average parameter of whole GaN core does not changed, while the increase of 2ThetaChi of $Ga_2O_3$ (020) in the Table 2 and the decrease of its parameter b, in Table 3, indicates the presence of a compressive $Ga_2O_3$ shell. For the specific case of thick $Ga_2O_3$ shell (> 10 nm), the compressive strain starts to be relaxed. In consequences, this partially relaxed shell induces tensile strain on the GaN-core.

**Table 3.** Parameter of crystals extracted from XRD measurements.

| | a of Si | a of GaN | b of $Ga_2O_3$ |
|---|---|---|---|
| T=900°C, $N_2/O_2$=5/1.3, Time=7min, Shell thickness=6.9 | 5.426 Å | 3.186 Å | 3.033 Å |
| T=850°C, $N_2/O_2$=5/1.3, Time=15min, Shell thickness=6.5 | 5.428 Å | 3.188 Å | 3.031 Å |
| T=850°C, $N_2/O_2$=5/0.8, Time=15min, Shell thickness=8.1 | 5.428 Å | 3.188 Å | 3.034 Å |
| Pure GaN NWs | 5.429 Å | 3.190 Å | |
| Theory parameter | 5.431 Å | 3.189 Å | 3.040 Å |

As shown on Figure 3, the peak of GaN (11-20) is very sharp, indicating uniform crystal parameter of GaN synthesized by PA-MBE. By contrast, the $Ga_2O_3$ (020) peak is quite broad and slightly shifted towards higher degrees. To explain these observations, we have to consider two phenomena:

1) Due to the stress undergone from GaN or due to the presence of possible defects at the GaN/$Ga_2O_3$ interface, the crystal parameter of $Ga_2O_3$ is varied in whole oxide shell. The variation of crystal parameter leads to the variation of 2ThetaChi, causing the wide peak in XRD spectra.

2) If we finely analyze the reference XRD spectra of β-$Ga_2O_3$ (Figure 3b), we can note the presence, very close to the $Ga_2O_3$ (020) peak, of the $Ga_2O_3$ (710) peak, with an estimated (from theoretical parameter) 2ThetaChi of 62.6294°. The widening of the $Ga_2O_3$ (020) and $Ga_2O_3$ (710) due to the crystalline non-homogeneity of the shell can lead to their overlap, then resulting in the appearance,

on XRD spectra, of a unique $Ga_2O_3$ (020) broad peak slightly shifted with respect to the peak theoretical position.

XRD evidence that the oxide shell synthesis by thermal treatment of MBE-grown GaN NWs leads to the formation of β-$Ga_2O_3$ crystalline phase. To further investigate the formation of this shell, we have analyzed some samples by XRD using in-plane Phi scan. In this configuration, the samples are rotated by 360° while the angle between the X-ray source and the detector (2ThetaChi) is fixed at 57.8°, 61.1° and 64.3° corresponding to GaN (11-20), β-$Ga_2O_3$ (020) and β-$Ga_2O_3$ (403). Figure 4 presents the results for pure GaN NWs and GaN/$Ga_2O_3$ NWs. On Figure 4a, six peaks respond to the six (11-20) planes of GaN, demonstrating the symmetry of hexagonal structure of GaN. Figure 4b, shows also six peaks, indicating that the (020) and (403) planes of β-$Ga_2O_3$ present symmetrically along the hexagonal structure of GaN. This result, in agreement with the result from Phi/2ThetaChi scan (Figure 3), demonstrates that the β-$Ga_2O_3$ synthesized by post-thermal treatment is grown in epitaxial relationship with the GaN core.

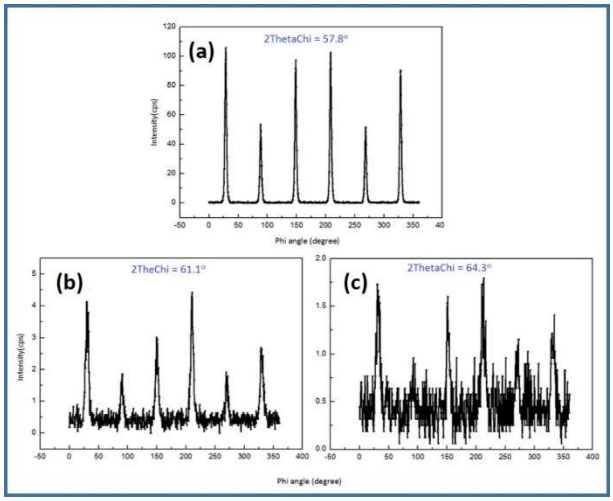


**Figure 4.** XRD analysis using in-plane Phi scan configuration of GaN/β-$Ga_2O_3$ NWs with the detector (2ThetaChi) fixed at 57.8° **(a)**, 61.1° **(b)** and 64.3° **(c)** corresponding to GaN (11-20), β-$Ga_2O_3$ (020) and β-$Ga_2O_3$ (403) respectively.

The XRD analysis have evidenced that the $Ga_2O_3$ shell crystallize in the β-$Ga_2O_3$, the most-stable phase, but is characterized by a lack of uniformity. To investigate this point, we have performed High-Resolved STEM analysis combined with EDX mapping. Figures 5a and 5c presents bright field and dark field images of GaN/β-$Ga_2O_3$ NWs. The crystal structure of the heterostructures is characterized by different patterns, corresponding to the structure of GaN for the core, and the structure of $Ga_2O_3$ oxide for the shell (of both sides of the NW). The TEM images evidence a ripple at the GaN/oxide interface and show variations in the shell lattice. This could be caused by the mismatch between GaN and $Ga_2O_3$ structures, creating internal stresses located in the shell, and the appearance of defects in $Ga_2O_3$.

The zoom in the NW core (figure 5c) indicates that the pattern responds to the (11-20) plane of hexagonal GaN. The perfect lattice of GaN in the figure indicates that its monocrystalline structure is preserved after the oxidation treatment. Concerning the shell, the TEM images reveal that it presents a different crystalline structure from the NW core and is non-uniform with different patterns. According to the result from XRD analysis, the plane (11-20) of GaN is parallel to the (020) plane of β-$Ga_2O_3$. This means the crystal structure of this plane, or of any other parallel ones, can be observed in the same images than one containing the (11-20) plane of GaN. Figure 5d presents STEM analysis performed at the GaN/ $Ga_2O_3$ interface. The shell presents the same structure than the structure of β-$Ga_2O_3$ (020) plane [60]. Combined with the fact that their parameters correspond to the theoretical ones, we can conclude that the oxide shell formed by thermal oxidation of MBE grown GaN NWs presents the monoclinic β-$Ga_2O_3$ crystalline phase [54]. The non-uniformity of the shell results from the mismatch caused by hexagonal structure of GaN, which disarranges the formation of monoclinic structure of $Ga_2O_3$ at the angles of hexagon. Since $Ga_2O_3$ structure has epitaxial relation with GaN

Peer-reviewed version available at *Appl. Sci.* **2019**, *9*, 3528; doi:10.3390/app9173528



structure, the angles of hexagonal structure change the direction of monoclinic structure in an inappropriate way for monoclinic structure, leading to the observed mixing direction of $Ga_2O_3$ lattice.

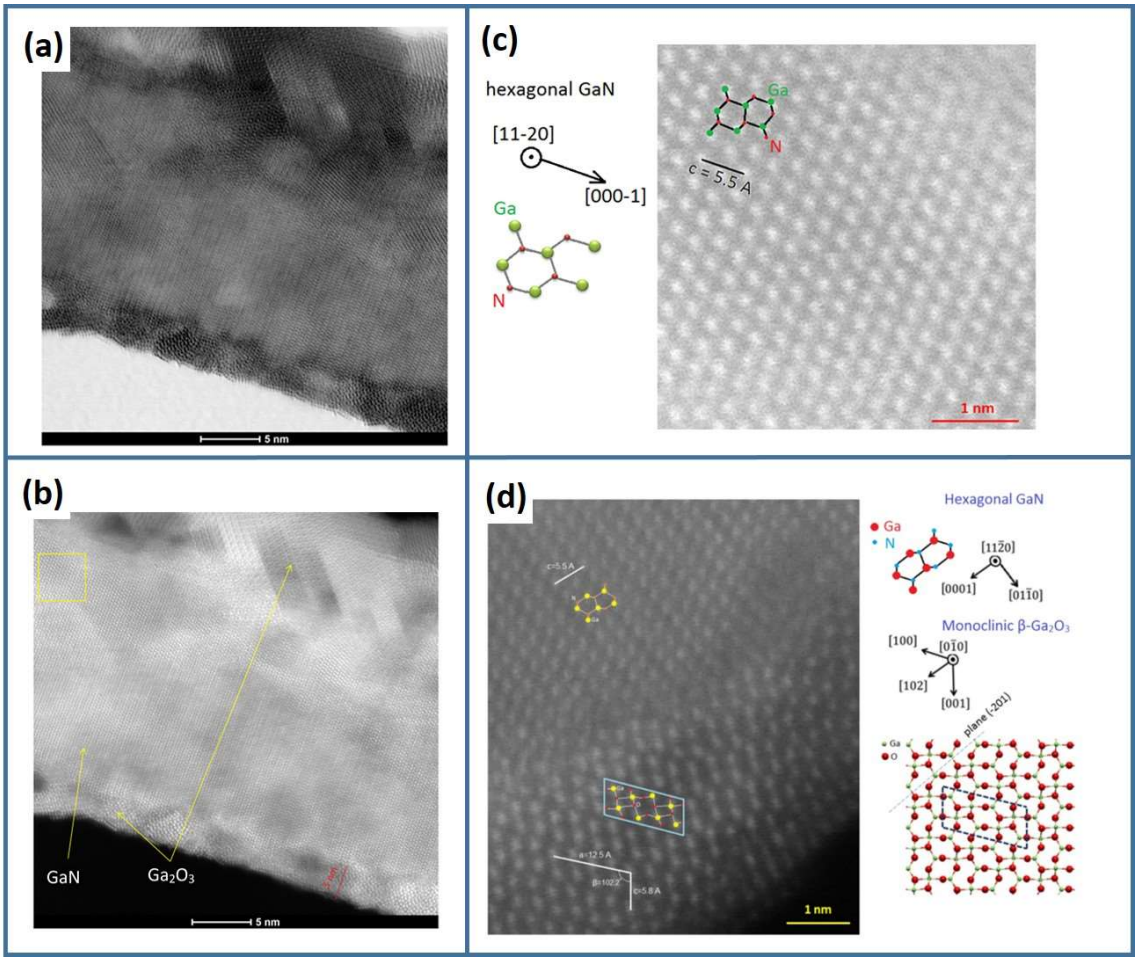


**Figure 5.** STEM images of GaN/$Ga_2O_3$ NWs in **(a)** bright field mode; **(b)** dark field mode. **(c)** Magnification of the GaN core. **(d)** Magnification at the GaN/$Ga_2O_3$ interface. The β-$Ga_2O_3$ structural representation is extracted from [54].

Finally, the Figure 6 presents EDX mapping performed on GaN/β-$Ga_2O_3$ NWs. The different elements composing the NW can be well distinguished between the GaN core and the $Ga_2O_3$ shell. At this stage, it is important to note that the blue dots of O atoms can be seen in an area of the GaN core. This is not the signature of oxygen contain inside the GaN core, but only the signature of a *visual effet*. In fact, because the $Ga_2O_3$ shell surrounds the GaN core, the electron beam is transmitted through the entire NWs, causing an overlaps of the core and shell signatures. The EDX mapping reveals that the β-$Ga_2O_3$ shell surrounds the wall GaN-core, which is of crucial importance to integrate this kind of heterostructures in gas-sensors. EDX mappings evidence also the border between the core and the shell, which expresses the ripple interface of GaN/$Ga_2O_3$ similar to ones observed by STEM. The thickness of the oxide shell extracted from EDX mapping is around 3-5 nm, this measurement being in good agreement with our estimations performed from SEM analyses (Figure 2).

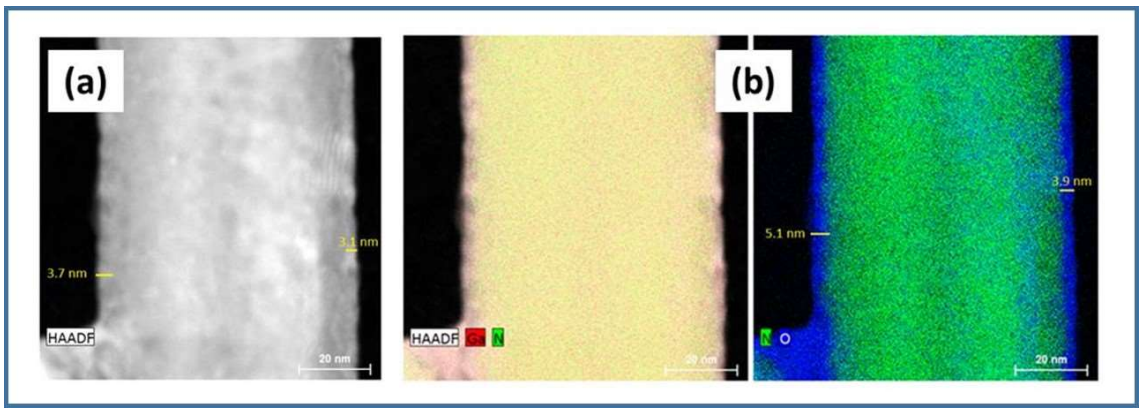


**Figure 6.** STEM **(a)** and EDX mappings **(b)** of GaN/$Ga_2O_3$ NW.

## 4. Conclusion

We have developped a synthesis procedure to form GaN/β-$Ga_2O_3$ NWs composed on two successive steps: (1) the growth of GaN NWs by plasma-assisted MBE, followed by (2) their thermal oxidation post-treatment, leading to the formation of a $Ga_2O_3$ shell surrounding the GaN-core. Due to the larger specific volume of $Ga_2O_3$ by regarding the one of GaN, the oxidation of the GaN-core is associated with an expansion of its diameter. We have analyzed the shell thickness variation (diameter expansion) as a function of the oxidation conditions (temperature, $O_2$ flux, atmosphere and time of oxidation). Then, we have established that the thickness of the $Ga_2O_3$ shell can be modulated with the oxidation conditions, from 1 up to 14 nm, and follows the diffuse-controlled reaction. The structural properties of the shell have been investigated by combining various techniques: XRD, TEM-STEM and EDX. We have demonstrated that the oxide shell formed by thermal oxidation is synthesized in epitaxial relationship with the GaN core. We have also established that the shell is crystalline and presents the β-Ga2O3 crystalline phase, the most stable one. By controlling the synthesis of GaN/β-$Ga_2O_3$ NWs, this paper constitutes a building block for developing high-efficient CO-gas sensors.

**Author Contributions:** "NW growth, M. Morassi, L. Travers, and Q.C. Bui.; Thermal oxidation, Q.C. Bui, X. Lafosse, and N. Gogneau.; Methodology, Q.C. Bui, M. Morassi and N. Gogneau.; NW structural characterizations, L. Largeau, Q. C. Bui, C. Dupuis, O. Mauguin, and N. Gogneau.; Investigation, Q.C. Bui, L. Largeau, and N. Gogneau.; Data Analysis, Q.C. Bui, M. Morassi, N. Jegenyes, L. Largeau, M. Tchernycheva, and N. Gogneau.; Validation, M. Tchernycheva, and N. Gogneau.; Funding Acquisition, M. Tchernycheva, J.C. Harmand, and N. Gogneau; Writing-Original Draft, Q.C. Bui, M. Tchernycheva, L. L.argeau, and N. Gogneau.; Supervision, M. Tchernycheva, J.C. Harmand, and N. Gogneau."

**Funding:** This work was financially supported by the French National Research Agency through the GANEX program (ANR-11-LABX-0014), and the EU Horizon 2020 ERC project 'NanoHarvest' (Grant 639052).

**Conflicts of Interest:** The authors declare no conflict of interest.

## References

1. Potyrailo, R. A. Multivariable Sensors for Ubiquitous Monitoring of Gases in the Era of Internet of Things and Industrial Internet. *Chem. Rev.* **2016**, *116*, 11877.
2. Shehzad, K.; Shi, T.; Qadir, A.; Wan, X.; Guo, H.; Ali, A.; Xuan, W.; Xu, H.; Gu, Z.; Peng, X.; Xie, J.; Sun, L.; He, Q.; Xu, Z.; Gao, C.; Rim, Y.-S.; Dan, Y.; Hasan, T.; Tan, P.; Li, E.; Yin, W.; Cheng, Z.; Yu, B.; Xu, Y.; Luo, J.; Duan, X. Designing an Efficient Multimode Environmental Sensor Based on Graphene–Silicon Heterojunction. *Adv. Mater. Technol.* **2017**, *2*, 1600262.
3. Shankar, P.; Bosco Balaguru Rayappan, J. Gas sensing mechanism of metal oxides: The role of ambient atmosphere, type of semiconductor and gases - A review. *Science Lett. J.* **2015**, *4*, 126.
4. Wang, C.; Yin, L.; Zhang, L.; Xiang, D.; Gao, R. Metal Oxide Gas Sensors: Sensitivity and Influencing Factors. *Sensors* **2010**, *10*, 2088.

5. Liua, Z.; Yamazakia, T.; Shena, Y.; Kikutaa, T.; Nakatania, N.; Li, Y. $O_2$ and CO sensing of $Ga_2O_3$ multiple nanowire gas sensors. *Sensors and Actuators B* **2008**, *129*, 666.
6. Fleischer, M.; Meixner, H. Electron mobility in single- and polycrystalline $Ga_2O_3$, *J. Appl. Phys.* **1993**, *74*, 300.
7. Mazeina, L.; Picard, Y. N.; Maximenko, S.I.; Perkins, F.K.; Glaser, E.R.; Twigg, M.E.; Freitas, J.A.; Prokes, S.M. Growth of Sn-Doped β-$Ga_2O_3$ Nanowires and $Ga_2O_3$-$SnO_2$ Heterostructures for Gas Sensing Applications. *Cryst. Growth & Des.* **2009**, *9*, 4471.
8. Bârsan, N.; Weimar, U. Understanding the fundamental principles of metal oxide based gas sensors; the example of CO sensing with $SnO_2$ sensors in the presence of humidity. *J. Phys.: Condens. Matter.* **2003**, *15*, R813.
9. Hahn, S.H.; Bârsan, N.; Weimar, U.; Ejakov, S.G.; Visser, J.H.; Soltis, R.E. CO sensing with $SnO_2$ thick film sensors: role of oxygen and water vapour. *Thin Solid Films* **2003**, *436*, 17.
10. Huang, J.; Wan Q. Gas Sensors Based on Semiconducting Metal Oxide One-Dimensional Nanostructures. *Sensors* **2009**, *9*, 9903.
11. Hernández-Ramírez, F.; Tarancón, A.; Casals, O. ; Arbiol, J. ; Morante, J. R. High response and stability in CO and humidity measures using a single $SnO_2$ nanowire. *Sensors and Actuators B* **2007**, *121*, 3.
12. Savagea, N.O.; Akbar, S.A.; Dutta, P.K. Titanium dioxide based high temperature carbon monoxide selective sensor. *Sensors and Actuators B: Chemical* **2001,** *72*, 239.
13. Fine, G.F.; Cavanagh, L.M.; Afonja, A.; Binions, R. Metal Oxide Semi-Conductor Gas Sensors in Environmental Monitoring. *Sensors* **2010**, *10*, 5469.
14. Oon, H.S.; Cheong,K. Y. Effect of Oxidation Time on Thermally Grown Oxide on GaN. *J. Mater. Eng. and Perf.* **2013**, *22*, 1341.
15. Korbutowicz, R.; Prazmowska, J. Wet Thermal Oxidation of GaAs and GaN. Semicond. Technol.,In *Jan Grym (Ed.)*, InTech (2010).
16. Hoefera, U.; Frank, J.; Fleischer, M. High temperature $Ga_2O_3$-gas sensor and $SnO_2$-gas sensors: a comparison. *Sensors and Actuators B* **2011**, *78*, 6.
17. Ogitaa, M.; Saikaa, N.; Nakanishi, Y.; Hatanaka, Y. $Ga_2O_3$ thin films for high-temperature gas sensors, *Appl. Surf. Sci.* **1999**, *142*, 188.
18. Schwebel, T.; Fleischer, M.; Meixner, H.; Kohl, C. D. CO-Sensor for domestic use based on high temperature stable $Ga_2O_3$ thin films. *Sensors and Actuators B*, **1998**, *49*, 46.
19. Korotcenkov, G. Metal oxides for solid-state gas sensors: What determines our choice? *Mater. Sci. Eng. B* **2007**, *139*, 1.
20. Franke, M. E.; Koplin, T. J.; Simon, U. Metal and metal oxide nanoparticles in chemiresistors: does the nanoscale matter? *Small* **2006**, *2*, 36.
21. Vander Wal, R. L.; Hunter, G. W.; Xu, J. C.; Kulis, M. J.; Berger, G. M.; Ticich, T. M. Metal-oxide nanostructure and gas-sensing performance. *Sens. Actuators B* **2009**, *138*, 113.
22. Jimerez-Cadena, G.; Riu, J.; Rius, F.X. *Analyst* **2007**, *132*, 1083.
23. Huang, X.-J.; Choi, Y.-K. Chemical sensors based on nanostructured materials. *Sens. Actuators B* **2007**, *122*, 659.
24. Comini, C. Metal oxide nano-crystals for gas sensing. *Anal. Chim. Acta* **2006**, *568*, 28.
25. Zhang, J.; Liu, X.; Neri, G.; Pinna, P. Nanostructured Materials for Room-Temperature Gas Sensors. *Adv. Mater*. **2016**, *28*, 795.
26. Chen, X.; Wong, C. K.; Yuan, C. A.; Zhang, G. Nanowire-based gas sensors. *Sens. Actuators B* **2013**, *177*, 178.
27. Ramgir, N. S.; Yang, Y.; Zacharias, M. Nanowire-based sensors. *Small* **2010**, *6*, 1705.
28. Devan, R. S.; Patil, R. A.; Lin, J. H.; Ma, Y. R. One-Dimensional Metal-Oxide Nanostructures: Recent Developments in Synthesis, Characterization, and Applications. *Adv. Funct. Mater.* **2012**, *22*, 3326.
29. Kolmakov, A.; Zhang, Y.; Cheng, G.; Koskovits, M. Detection of CO and O2 Using Tin Oxide Nanowire Sensors.*Adv. Mater.* **2003**, *15*, 997.
30. Yang, P.; Yan, R.; Fardy, M. Semiconductor nanowire: what's next? *Nano Lett.* **2010**, *10*, 1529.
31. Cao, G. In *Nanostructures and Nanomaterials*, Imperial Collage Press. London, 2004
32. Miller, D. R. ; Akbar, S. A.; Morris, P. A. Nanoscale metal oxide-based heterojunctions for gas sensing: A review. *Sens. Actuators, B* **2014** , *204* , 250.
33. Willinger, M-G; Neri, G.; Rauwel, E.; Bonavita, A.; Micali, G.; Pinna, N. Vanadium Oxide Sensing Layer Grown on Carbon Nanotubes by a New Atomic Layer Deposition Process. *Nano. Lett.* **2008**, *8*, 4201.

34. Jang, Y-G; Kim, W-S.; Kim, D-H.; Hong, S-Y. Fabrication of $Ga_2O_3/SnO_2$ core–shell nanowires and their ethanol gas sensing properties, *J. Mater. Res.* **2011**, *26*, 2322.
35. Liu, Y.; Zhu, G.; Chen, J.; Xu, H.; Shen, X.; Yuan, A. $Co_3O_4$/ZnO nanocomposites for gas-sensing applications. *Appl. Surf. Sci.* **2013**, *265*, 379.
36. Lai, H.-Y. ; Chen, C.-H. ; Highly sensitive room-temperature CO gas sensors: Pt and Pd nanoparticle-decorated $In_2O_3$ flower-like nanobundles. *J. Mater. Chem.* **2012** , *22* , 13204.
37. Park, S. H.; Kim, S.H.; Park, S. Y.; Lee, C. Synthesis and CO gas sensing properties of surface nitridated $Ga_2O_3$ nanowires. *RSC Adv.* **2014**, *4*, 63402.
38. Korotcenkov, G. Metal oxides for solid-state gas sensors: What determines our choice? *Materials Science and Engineering: B* **2007**, *139*, 1.
39. Prasad, R. M.; Lauterbach, S.; Kleebe, H-J.; Merdrignac-Conanec, O.; Barsan, N.; Weimar, U.; Gurlo, A. Response of Gallium Nitride Chemiresistors to Carbon Monoxide is Due to Oxygen Contamination. *ACS Sens.* **2017**, *2*, 713
40. Largeau, L.; Galopin, E.; Gogneau, N.; Travers, L.; Glas, F.; Harmand, J-C. N-Polar GaN Nanowires Seeded by Al Droplets on Si(111). *Cryst. Growth Des.* **2012**, 12, 2724
41. Brubaker, M. D.; Levin, I.; Davydov, A.V.; Rourke, D. M.; Sanford, N. A.; Bright, V. M.; and Bertness, K. A. GaN based nanorods for solid state lighting. *J. Appl. Phys.* **2011**, 110, 053506
42. Songmuang, R.; Landré, O.; and Daudin, B. Molecular beam epitaxy growth and optical properties of AlN nanowires. *Appl. Phys. Lett.* **2007**, 91, 251902
43. Bertness, K. A.; Roshko, A.; Mansfield, L. M.; Harvey, T. E.; and Sanford, N. A. Nucleation conditions for catalyst-free GaN nanowires. First International Symposium on Growth of Nitrides. *J. Cryst. Growth* **2007**, 300, 94
44. Largeau, L.; Dheeraj, D. L.; Tchernycheva, M.; Cirlin, G. E.; Harmand, J. C. Facet and in-plane crystallographic orientations of GaN nanowires grown on Si(111). *Nanotechnology* **2008**, *19*, 155704.
45. Largeau, L.; Galopin, E.; Gogneau, N.; Travers, L.; Glas, F.; Harmand, JC. N-Polar GaN Nanowires Seeded by Al Droplets on Si(111)C. *Cryst. Growth Des.* **2012**, *12*, 2724.
46. Auzelle, T.; Haas, B.; Minj, A.; Bougerol, C.; Rouvière, J.-L.; Cros, A.; Colchero, J.; Daudin, B. The influence of AlN buffer over the polarity and the nucleation of self-organized GaN nanowires. *J. Appl. Phys.* **2015**, *117*, 245303.
47. Parameters of semiconductor. Retrieved from http://www.ioffe.ru/SVA/NSM/Semicond
48. Gallium(III) Oxide. Retrieved from http://www.sigmaaldrich.com/catalog/product/aldrich/215066
49. Yamada, T.; Ito, J.; Asahara, R.; Watanabe, K.; Nozaki, M.; Nakazawa, S.; Anda, Y.; Ishida, M.; Ueda, T.; Yoshigoe, A.; Hosoi, T.; Shimura, T.; Watanabe, H. Comprehensive study on initial thermal oxidation of GaN(0001) surface and subsequent oxide growth in dry oxygen ambient. *J. Appl. Phys.* **2017**, *121*, 035303.
50. Chen, P.; Zhang, R.; Xu, X.F.; Zhou, Y.G.; Chen, Z.Z.; Xie, S.Y.; Li, W.P.; Zheng, Y.D. The oxidation of gallium nitride epilayers in dry oxygen, *Appl. Phys. A* **2000**, *71*, 191.
51. Wolter S. D.; Mohney, S. E.; Venugopalan, H.; Wickenden, A. E.; Koleske, D. D. Kinetic Study of the Oxidation of Gallium Nitride in Dry Air. *J. Electrochem. Soc.* **1998**, *145*, 629.
52. Zhou, Y.; Ahyia, C.; Isaacs-Smith, T.; Bozack, M.; Tina, C-C.; illiams, J.; Park, M.; Cheng, A-J.; Park, J-H.; Kim, D-J.; Wang, D.; Preble, E.A.; Hanser, A.; Evans, K. Formation, etching and electrical characterization of a thermally grown gallium oxide on the Ga-face of a bulk GaN substrate. *Solid-State Electronics* **2008**, *52*, 756.
53. Li, Y.; Tokizono, T.; Liao, M.; Zhong, M.; Koide, Y.; Yamada, I.; Delaunay, J.J. Efficient Assembly of Bridged β-Ga2O3 Nanowires for Solar-Blind Photodetection. *Adv. Func. Mater.* **2010**, *20*, 3972.
54. Hanada, K.; Moribayashi, O.; Koshi, K.; Sasaki, K.; Kuramata, A.; Ueda, O.; Kasu, M. Origins of etch pits in β-$Ga_2O_3$(010) single crystals. *Japan. J. Appl. Phys.* **2016**, *55*, 1202BG.